First-principles study of PbTiO₃ under uniaxial strains and stresses

Henu Sharma,[1,2,3] Jens Kreisel,[3,4] and Philippe Ghosez[1]

[1]*Physique Théorique des Matériaux, Université de Liège, B-4000 Sart Tilman, Belgium*
[2]*Laboratoire des Matériaux et Génie Physique, Grenoble INP-CNRS, Grenoble, France*
[3]*Département Science et Analyse des Matériaux, Centre de Recherche Public Gabriel Lippmann, 41 Rue du Brill, L-4422 Belvaux, Luxembourg*
[4]*Physics and Materials Science Research Unit, University of Luxembourg, 41 Rue du Brill, L-4422 Belvaux, Luxembourg*

The behavior of PbTiO₃ under uniaxial strains and stresses is investigated from first-principles calculations within density functional theory. We show that irrespective of the uniaxial mechanical constraint applied, the system keeps a purely ferroelectric ground state, with the polarization aligned either along the constraint direction (FE$_z$ phase) or along one of the pseudocubic axes perpendicular to it (FE$_x$ phase). This contrasts with the cases of isotropic and biaxial mechanical constraints for which novel phases combining ferroelectric and antiferrodistortive motions have been previously reported. Under uniaxial strain, PbTiO₃ switched from an FE$_x$ ground state under compressive strain to an FE$_z$ ground state under tensile strain beyond a critical strain $\eta_{zz}^c \approx +1\%$. Under uniaxial stress, PbTiO₃ exhibits either an FE$_x$ ground state under compression ($\sigma_{zz} < 0$) or an FE$_z$ ground state under tension ($\sigma_{zz} > 0$). Here, however, an abrupt jump of the structural parameters is also predicted under both compressive and tensile stresses at critical values $\sigma_{zz} \approx +2$ and -8 GPa. This behavior appears to be similar to that predicted under negative isotropic pressure and might turn out to be practically useful for enhancing the piezoelectric response in nanodevices.

PACS number(s): 61.50.Ks, 77.84.−s, 31.15.A−

I. INTRODUCTION

ABO_3 perovskites form a very important class of functional materials that can exhibit a broad range of properties (e.g., superconductivity, magnetism, ferroelectricity, multiferroism, and metal-insulator transitions) within small distortions of the prototype cubic structure. Among them, PbTiO₃ is a prototypical ferroelectric compound and also one of the parent components of the Pb(Zr,Ti)O₃ solid solution (PZT), which is the most widely used piezoelectric [1].

Bulk PbTiO₃ crystallizes at high temperature in the paraelectric $Pm\bar{3}m$ cubic structure. Under cooling, it then undergoes, at 760 K, a structural phase transition to a ferroelectric (FE) phase of $P4mm$ symmetry. At room temperature, it possesses a large spontaneous polarization $P_s \approx 80$ μC/cm². In contrast to BaTiO₃ and KNbO₃, which exhibit additional ferroelectric transitions to phases of orthorhombic and rhombohedral symmetries, PbTiO₃ remains tetragonal down to 0 K, a feature that was attributed to its large c/a ratio [2]. As revealed by the inspection of the phonon dispersion curves of its cubic phase [3], on top of its ferroelectric instability, PbTiO₃ also develops strong antiferrodistortive (AFD) instabilities, which are associated with rotations (tilts) of the oxygen octahedra. Although these AFD instabilities are suppressed by the appearance of the dominant FE motions, they nevertheless constitute important hidden instabilities that can significantly affect its physical and structural properties. For instance, it was recently highlighted theoretically that AFD motions shift down the ferroelectric phase-transition temperature of PbTiO₃ by a few hundred Kelvin [4]. Also, although they do not naturally appear in bulk, AFD motions can condense at the PbTiO₃ surface [5] where the FE-AFD competition is modified.

In ABO_3 compounds, FE and AFD instabilities are highly sensitive to mechanical constraints such as strains and stresses, which can thus be used in practice to tune the phase-transition temperatures and the multifunctional properties [1]. Under increasing *isotropic* pressure, the ferroelectric instability is well known for disappearing quickly, an intrinsic feature that has to be properly handled when doing first-principles calculations within the local-density approximation, which tends to underestimate systematically bond lengths and unit-cell volumes [6]. Unexpectedly, in PbTiO₃, Kornev *et al.* [7] showed that, although ferroelectricity is indeed progressively suppressed at low isotropic pressure, it reappears at ultrahigh pressure, a feature also predicted in BaTiO₃ [8]. Following this work the phase diagram of PbTiO₃ under isotropic pressure has recently been reinvestigated by Janolin *et al.* [9]: they highlighted a complex sequence of phases accommodating pressure through mechanisms involving not only the reentrance of ferroelectricity but also oxygen octahedra tilting, which are known to be favored at smaller volumes.

Engineering ferroelectricity through *biaxial* epitaxial strain in ABO_3 thin films has also attracted much attention over the last decade [10–12]. Thanks to the advances in the deposition of coherent epitaxial films of complex oxides [13], it has become possible to impose epitaxial strains of the order of 4% or even larger to thin-film perovskites. It is now well understood that the substrate-induced biaxial strain has a strong bearing on the ultimate behavior of ferroelectric thin films [14–16]. Prototypical demonstrations of this include the strong amplification of ferroelectricity in strained BaTiO₃ [17] and the possibility to achieve room-temperature ferroelectricity in strained SrTiO₃ [18,19]. Such behaviors were predicted by Landau theory [14,15] and were further analyzed from first-principles investigations [16]. Strain engineering of ferroelectricity was also considered to be a promising route to convert paraelectric magnets into multiferroics [20], for instance, in CaMnO₃ [21,22] and is not restricted to perovskites [23]. Beyond acting simply on the ferroelectric mode as initially targeted, strain engineering also proved to be useful for tuning the competition with other instabilities and getting novel unexpected phases such as in BiFeO₃ under

either in-plane compressive [24,25] or tensile [26] strains or in EuTiO$_3$ [27] and SrMnO$_3$ [28] in combination with magnetism. In PbTiO$_3$ it was predicted from first-principles that, while moderate compressive strain will favor the $P4mm$ ferroelectric phase and amplify the spontaneous polarization, tensile epitaxial strain should favor an $Ima2_1$ phase [29–31] combining in-plane FE polarization (along the [110] direction) and in-plane AFD oxygen rotations ($a^-a^-c^0$ in Glazer's notation [32,33]). Additional $I4cm$ and $Pmc2_1$ phases have also been predicted at larger compressive and tensile strains, respectively [31].

While the effect of isotropic and biaxial mechanical constraints on the ferroelectric properties has been widely investigated, our study is motivated by the little-understood effect of *uniaxial* strain and stress. Emelyanov *et al.* discussed, using a thermodynamical theory, the additional effect of uniaxial stress produced by uniform loading of epitaxial thin films of BaTiO$_3$ and PbTiO$_3$ under biaxial strain [34]. Also, the role of uniaxial strain on PbTiO$_3$ ultrathin slabs has been studied by Umeno *et al.* from first principles [35]; they reported the possibility to observe a combination of FE and AFD distortions, although the appearance of the latter might result from a surface, rather than a purely strain, effect. More recently, Duan *et al.* [36] investigated the role of uniaxial stress on bulk PbTiO$_3$, but they did not consider the possible interplay between ferroelectricity and AFD motions; moreover, as will become more clear below, their conclusions are biased by the fact that they restricted themselves to a particular phase.

Within our work, we want to study more systematically the role of uniaxial mechanical constraints in monodomain PbTiO$_3$, clarifying if it leads to a suppression of FE in favor of AFD distortions or if FE structures are favored at any uniaxial strain or stress state. We wish to explore if uniaxial strain or stress can lead to new structures in PbTiO$_3$; we are motivated by the fact that perovskites with competing FE and AFD instabilities can show a multitude of structures under deformation, as observed not only under biaxial or isotropic constraints for in PbTiO$_3$ but also under biaxial strain for BiFeO$_3$ [24] and under hydrostatic pressure for BiFeO$_3$ [37] and BiMnO$_3$ [38]. To do so, we perform first-principles calculations within density functional theory in order to determine the ground state of PbTiO$_3$ under uniaxial strains and stresses.

II. TECHNICAL DETAILS

Our first-principles calculations have been performed in the framework of density functional theory (DFT) as implemented in the ABINIT package [39–41]. We did calculations using both (i) the local-density approximation (LDA) [42] and extended norm-conserving Teter pseudopotentials [43] and (ii) the generalized gradient approximation with the functional proposed by Wu and Cohen (GGA-WC) [44] and optimized pseudopotentials [45] generated with the OPIUM code [46]. In both cases, semicore states were treated as valence electrons, considering explicitly the following levels in the calculation: $5s$, $5p$, and $6s$ for the Pb atom, $3s$, $3p$, $3d$, and $4s$ for the Ti atom, and $2s$ and $2p$ for the O atom. The wave function was expanded on a plane-wave basis set. Convergency was reached using a plane-wave energy cutoff of 45 hartrees.
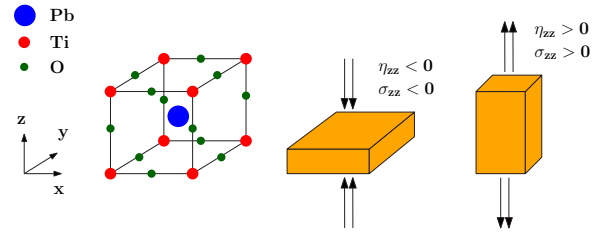

FIG. 1. (Color online) Cubic perovskite structure of PbTiO$_3$, with the Ti atom at the origin. Pb atoms are located at the center (in blue), Ti atoms are at the corners (in red), and O atoms are at the middle of the edges (in green). The uniaxial mechanical constraint (fixed strain η_{zz} or fixed stress σ_{zz}) is applied along the z axis.

In the five-atom perovskite ABO_3 unit cell, a Monkhorst-Pack mesh of $6 \times 6 \times 6$ k points was used to sample the Brillouin zone. When condensing the AFD instabilities, we considered either a 20-atom supercell corresponding to $\sqrt{2}a_0 = a = b$ and $c = 2a_0$ and a sampling of $6 \times 6 \times 4$ k points or, for the $Cmcm$ phase, a 40-atom supercell corresponding to $2a_0$, $2a_0$, and $2a_0$ and a sampling of $4 \times 4 \times 4$ k points. We explicitly checked that the relative energy of the different phases is well converged and independent of the choice of the supercell. Structural relaxations were performed until the forces were smaller than 10^{-7} hartrees/bohr and stresses were smaller than 10^{-8} hartrees/bohr^3. The vibrational properties, Born effective charges, and dielectric tensors were calculated using the density functional perturbation theory (DFPT) [47]. The spontaneous polarizations were computed using the Berry phase formalism [48].

In what follows, we consider that the x, y, and z Cartesian axes are aligned with cell vectors a, b, and c of the reference cubic structure, respectively. Then, the uniaxial constraint is always applied along the z direction, as illustrated in Fig. 1. Both fixed uniaxial strain and fixed uniaxial stress conditions will be considered.

To label the ferroelectric and antiferrodistortive motions compatible with a given space group, we use "extended" Glazer's notation in which the superscripts refer, as usual, to the rotation pattern and a subscript P is added to identify the direction(s) along which a polarization can develop. When reporting phonon labels, we consider that the Ti atom is at the origin.

III. BULK STRUCTURE

First, we reinvestigate the highly symmetric cubic perovskite structure of PbTiO$_3$. In this cubic phase, the atomic positions are fixed by symmetry, and the only structural parameter to be relaxed is the lattice constant a_0. Our relaxed lattice constants $a_0^{LDA} = 3.880$ Å and $a_0^{GGA} = 3.933$ Å are comparable to previous calculations ($a_0^{LDA} = 3.874$ Å [36]) and are in satisfactory agreement with experimental data ($a_0^{EXP} = 3.93$ Å [49]). As expected, the LDA tends to underestimate the experimental lattice constant, which is better reproduced at the GGA-WC level.

The calculated phonon dispersion curves of cubic PbTiO$_3$ (not shown here) are also in agreement with previous studies [3]. They show two main phonon instabilities: (i) a

TABLE I. Cell parameters, internal energies, and distortion amplitudes of different metastable phases of PbTiO$_3$ fully relaxed within the LDA and the GGA-WC (values in parentheses). For each phase, we specify the space group and, in parentheses, the compatible FE and AFD structural distortion using generalized Glazer's notation (see Sec. II). The amplitudes of the spontaneous polarization (P_s) and of the oxygen octahedra rotation angle (ϕ) are reported when appropriate. For the $Pm\bar{3}m$ and $P4mm$ phases, the experimental parameters (Exp.) are reported for comparison.

| Phase | Unit cell | | | Energy | Distortion |
	a (Å)	b (Å)	c (Å)	ΔE (meV/f.u.)	angle (deg) or P_s (μC/cm^2)
$Pm\bar{3}m$	3.880	3.880	3.880	0	
$(a^0a^0a^0)$	(3.935)	(3.935)	(3.935)	(0)	
Exp. [49]	3.93	3.93	3.93		
$P4mm$	3.863	3.863	3.975	-36.70	$P_s = 70$
$(a^0a^0c_P^0)$	(3.880)	(3.880)	(4.243)	(-83.27)	$(P_s = 97)$
Exp. [50]	3.880	3.880	4.155		$P_s = 75$
$Amm2$	3.912	3.912	3.865	-31.60	$P_s = 63$
$(a_P^0a_P^0c^0)$	(3.999)	(3.999)	(3.901)	(-62.90)	$(P_s = 75)$
$R3m$	3.895	3.895	3.895	-30.02	$P_s = 62$
$(a_P^0a_P^0a_P^0)$	(3.962)	(3.962)	(3.962)	(-58.25)	$(P_s = 71)$
$P4/mbm$	5.477	5.477	7.783	-3.20	$\phi^+ = 4.13$
$(a^0a^0c^+)$	(5.558)	(5.558)	(7.880)	(-1.06)	$(\phi^+ = 3.09)$
$I4/mcm$	5.470	5.470	7.797	-10.80	$\phi^- = 5.62$
$(a^0a^0c^-)$	(5.552)	(5.552)	(7.891)	(-5.00)	$(\phi^- = 4.60)$
$Imma$	5.480	5.505	7.732	-12.01	$\phi^- = 4.15$
$(a^-a^-c^0)$	(5.559)	(5.576)	(7.850)	(-5.59)	$(\phi^- = 3.43)$
$R\bar{3}c$	7.756	7.756	7.756	-12.00	$\phi^- = 3.36$
$(a^-a^-a^-)$	(7.866)	(7.866)	(7.866)	(-5.29)	$(\phi^- = 2.7)$

zone-center FE unstable mode Γ^{4-} (F_{1u}) at $109i$ ($151i$) cm^{-1} in LDA (GGA-WC) corresponding to a polar displacement of cations against the oxygen and (ii) a zone-boundary AFD unstable mode R^{4+} at $98i$ ($79i$) cm^{-1} in LDA (GGA-WC) corresponding to rotations of the oxygen octahedra, with consecutive octahedra along the rotation axis moving antiphase (a^- in Glazer's notation). As usual in perovskites, we notice that the AFD instability at the R point propagates to the M point through a M^{3+} mode at $73i$ ($53i$) cm^{-1} in LDA (GGA-WC), where consecutive octahedra move in phase (a^+ in Glazer's notations). The main difference between the LDA and GGA-WC results comes from the smaller LDA volume, which favors the AFD instabilities and reduces the FE instability.

From this discussion, it appears that, at the harmonic level, the FE instability is stronger than the AFD instabilities. However, this does not necessarily imply a FE ground state. In Table I, we report the energy and structural parameters of different metastable phases resulting from the condensation of the FE mode at Γ and AFD modes at R and M points. Both LDA and GGA-WC correctly reproduce the $P4mm$ ferroelectric ground state. We see that in the absence of FE instability, PbTiO$_3$ would prefer to develop a^- rotation patterns and would adopt either the $Imma$ ($a^-a^-c^0$) phase or the $R\bar{3}c$ ($a^-a^-a^-$) phase, which both appear to be nearly degenerated in energy in our calculations (i.e., with a difference
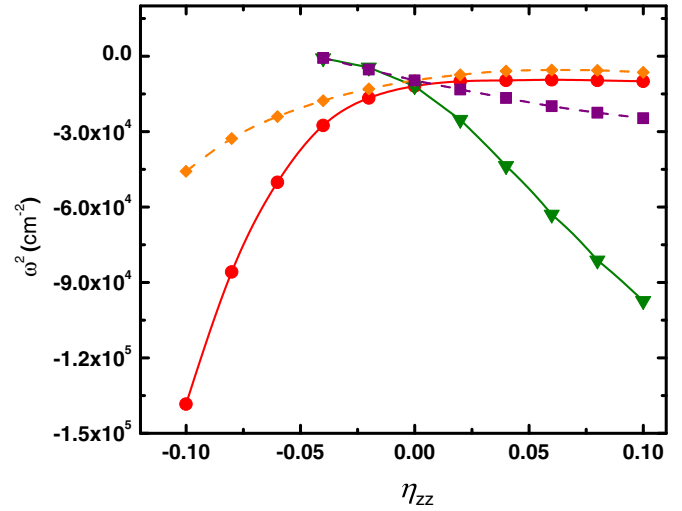

FIG. 2. (Color online) Evolution of the square of the frequency of the FE modes Γ^{3-} (green triangles) and Γ^{5-} (red circles) and of the AFD modes A_3^+ (purple squares) and A_5^+ (orange diamonds) with uniaxial strains in the paraelectric $P4/mmm$ phase of PbTiO$_3$, as obtained within the LDA. Similar results have been obtained within the GGA-WC.

of energy smaller than 1 meV/f.u.). The $I4/mcm$ ($a^0a^0c^-$) phase is also very close in energy. In comparison, the a^+ rotation pattern never produces a substantial gain in energy; in line with this, we notice that atomic relaxations in the $Cmcm$ ($a^0b^+c^-$) and $Pbnm$ ($a^-a^-c^+$) symmetries relax back to the $I4/mcm$ and $Imma$ phases, respectively, proving that the appearance of the a^- rotation suppresses the instability associated with a^+ motions.

Applying uniaxial strain along the z direction and relaxing the lattice constant along the two other directions while keeping the atoms at their high-symmetry position make the paraelectric reference unit cell tetragonal, bringing the system from $Pm\bar{3}m$ to $P4/mmm$ symmetry. This splits the triply degenerated Γ^{4-} (F_{1u}) FE mode into a single Γ^{3-} (A_1) mode and a doubly degenerated Γ^{5-} (E) mode, polarized along the c axis and perpendicular to it, respectively. Similarly, the triply degenerated R^{4+} AFD mode is split into a single A_3^+ mode and a doubly degenerated A_5^+ mode, corresponding to oxygen rotations around the z axis and around the x and y axes, respectively. The evolution of the frequencies of these modes with uniaxial strain is reported in Fig. 2. It appears that while the FE instability is only marginally more unstable than the AFD instability at the bulk level, both tensile and compressive uniaxial strains destabilize one of the FE modes (Γ^{3-} under tension and Γ^{5-} under compression) more strongly than any of the AFD ones. Although limited to the harmonic level, this observation already suggests that the behavior of PbTiO$_3$ under uniaxial mechanical constraints is strongly dominated by the FE instability.

IV. UNIAXIAL STRAIN

Let us now focus on the behavior of PbTiO$_3$ under uniaxial strain. The mechanical constraint is applied along the z axis by fixing the c lattice parameter. Then, structural relaxations

FIG. 4. (Color online) Evolution of the c/a ratio of the relaxed FE$_x$ ($Pmm2$) and FE$_z$ ($P4mm$) phases of PbTiO$_3$ with the uniaxial strain as obtained in LDA.
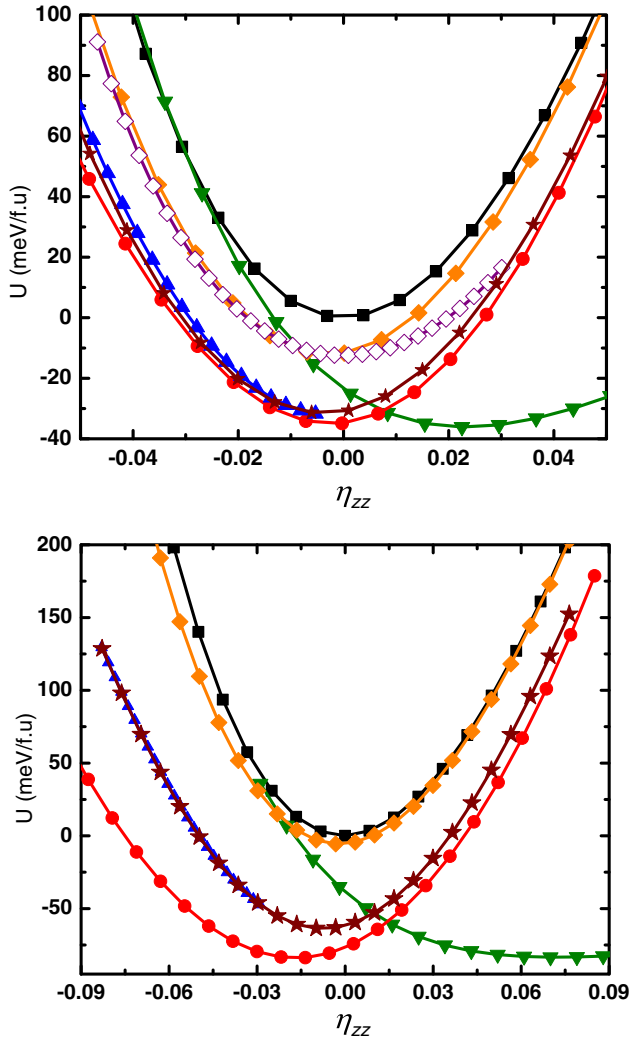

FIG. 3. (Color online) Internal energy U (meV/f.u.) of different metastable phases of PbTiO$_3$ under uniaxial strain as computed within (a) the LDA and (b) the GGA-WC. The phases are as follows: PE ($P4/mmm$, black squares), FE$_z$ ($P4mm$, green downward triangles), FE$_{xy}$ ($Amm2$, blue triangles), FE$_x$ ($Pmm2$, red circles), AFD$_{xy}$ (orange diamonds), AFD$_{xyz}$ (open purple diamonds), and AFD$_{xy}$ + FE$_{xy}$ (brown stars).

are performed under different symmetry constraints in order to compare the stability of different metastable phases for different amplitudes of the strain η_{zz}. The most stable phase at a given η_{zz} is that which minimizes the internal energy U. The results obtained in LDA are summarized in Fig. 3(a), and GGA-WC results are given in Fig. 3(b). In the following, we will mostly refer to LDA results, unless a further consideration of GGA-WC is pertinent.

The relaxed $Pm\bar{3}m$ cubic phase of PbTiO$_3$ has a lattice constant $a^{\text{LDA}} = 3.880$ Å ($a^{\text{GGA}} = 3.935$ Å) and is chosen to be the common reference for both the internal energy ($U = 0$) and the strain [$\eta_{zz} = (c - c_0)/c_0$ with $c_0 = a^{\text{LDA}}$ or a^{GGA}].

Applying a strain η_{zz} to the paraelectric $Pm\bar{3}m$ phase while keeping the atoms at their high-symmetry positions brings the system into the $P4/mmm$ symmetry (black squares in Fig. 3). As highlighted in the previous section, this paraelectric (PE) phase is not the ground state: it exhibits different FE and AFD
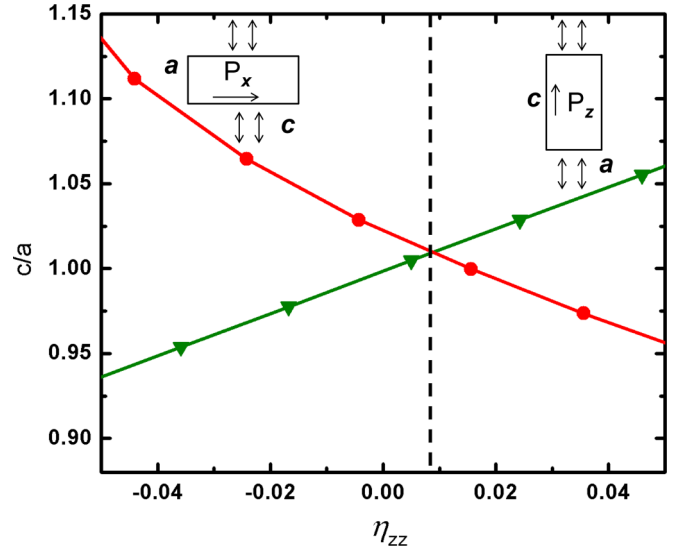
instabilities, the condensation of which will necessarily lower the internal energy.

Distinct polar phases, with their polar axes aligned along different directions, have been relaxed. They are labeled FE$_z$ ($P4mm$), FE$_x$ ($Pmm2$), or FE$_{xy}$ ($Amm2$) depending on whether the polar axis is along the [001], [100], or [110] direction, respectively [51]. We see in Fig. 3 that the FE$_z$ and FE$_x$ curves have their minima at the same internal energy for a value of strain associated in LDA (GGA-WC) to $c = 3.975$ Å (4.243 Å) and $a = 3.863$ Å (3.880 Å), which correspond to the c and a relaxed lattice constants of the bulk $P4mm$ ground state. The relative position of these two curves is such that the FE$_x$ phase appears to be the most stable for $\eta_{zz} < +0.8\%$, while the FE$_z$ phase is favored under tensile strains $\eta_{zz} > 0.8\%$. In Fig. 4 we have plotted the c/a ratio of the FE$_z$ and FE$_x$ phases: we see that the crossing of the two curves coincides with the change in stability of the two phases, emphasizing that PbTiO$_3$ prefers, at each strain, the phase that maximizes its c/a ratio.

We notice also in Fig. 3 that, contrary to what was proposed in Ref. [36], the paraelectric configuration is never the most stable. In agreement with that work, we see in Fig. 5(a) that PbTiO$_3$ cannot sustain a spontaneous polarization along z under large compressive strain $\eta_{zz} < -2.5\%$ (i.e., the $P4mm$ curve coincides with the $P4/mmm$ curve for $\eta_{zz} < -2.5\%$), but the system does not become paraelectric: instead, it prefers to stay ferroelectric and to develop a polarization in the perpendicular direction ($Pmm2$ phase). Under both tensile and compressive strains, the polarization is typically enhanced compared to the bulk value (Fig. 5).

Independently, we also considered different possible phases including AFD motions. According to what was discussed for the bulk, we only considered the most favorable a^- AFD motions. The AFD$_{xy}$ ($Imma$) and AFD$_{xyz}$ ($C2/c$) phases are compatible with the rotation patterns $a^-a^-c^0$ and $a^-a^-c^-$, respectively. The strain evolution of the relaxed rotation angles
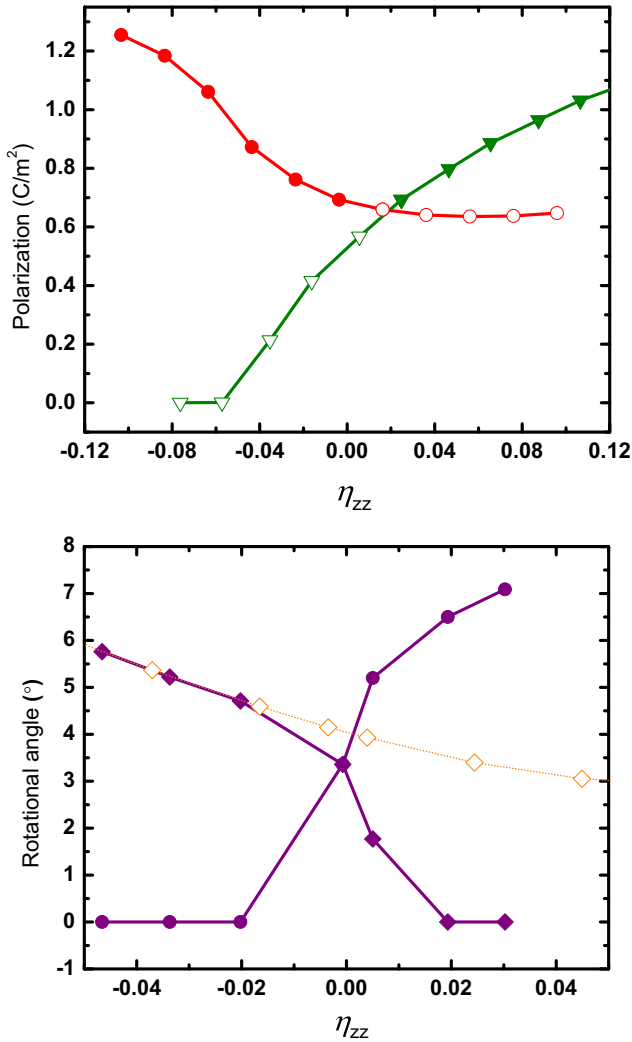
FIG. 5. (Color online) (top) Evolution of the polarization of the FE$_x$ (red circles) and FE$_z$ (green triangles) phases of PbTiO$_3$ with the uniaxial strain, as predicted within the LDA. Solid symbols correspond to the region where the phase is the ground state [52]. (bottom) Evolution of the rotational angles of the AFD$_{xy}$ and AFD$_{xyz}$ phases of PbTiO$_3$ with the uniaxial strain, as predicted within the LDA. Purple solid circles and diamonds indicate c^- and a^- rotation angles of the AFD$_{xyz}$ phases, respectively, and orange open diamonds indicate a^- rotation angles of the AFD$_{xy}$ phases.

of both phases are shown in Fig. 5. We observe that the relaxed AFD$_{xyz}$ phase only combines rotations along the three Cartesian directions in a small region of strain, around $\eta = 0$: under tensile strain, it prefers a purely $a^0a^0c^-$ rotation pattern, while under compressive strain, it prefers a purely $a^-a^-c^0$ rotation pattern (i.e., it reduces to the AFD$_{xy}$ phase). In all cases, the gain of energy produced by the AFD motions is much smaller than what can be obtained from the polar distortion.

It is also worth noticing in Fig. 3 that, like at the bulk level, the polarization always prefers to stay aligned with one of the pseudocubic axes (z or x) and that the FE$_{xy}$ phase is never the most stable. Nevertheless, its energy is very close to that of the FE$_x$ phase. In contrast, under compressive uniaxial strain, for which lattice constants perpendicular to the

constrained direction are elongated, the FE$_{xy}$ phase develops an AFD instability. This instability is associated with the $a^-a^-c^0$ AFD motions of the AFD$_{xy}$ phase, which appears to be the most favorable AFD configuration under compressive strain. Condensing these additional AFD motions in the FE$_{xy}$ phase brings the system into a FE$_{xy}$ + AFD$_{xy}$ phase ($a_P^-a_P^-c^0$ in generalized Glazer's notation) of $Ima2_1$ symmetry that is lower in energy than the purely FE$_{xy}$ phase but is never more stable than the FE$_x$ phase. This result is in contrast to the prediction of an $Ima2_1$ ground state for PbTiO$_3$ under tensile epitaxial biaxial strain [29–31]. The difference in behavior can be explained by the fact that the biaxial tensile strain forces two elongated lattice constants to be equal, favoring a FE$_{xy}$ + AFD$_{xy}$ distortion, while under uniaxial compressive strain, the lattice constants in the two directions perpendicular to the constraint are similarly elongated but the system keeps the freedom to break the symmetry between them.

We see in Fig. 3(b) that the gains in energy associated with the FE distortions are amplified and those associated with AFD motions are significantly reduced with the GGA-WC in comparison to the LDA. Still, the system switches from a FE$_x$ ground state to a FE$_z$ ground state at a relatively similar critical strain, $\eta_{zz} = 1.5\%$.

In summary, under uniaxial strain, PbTiO$_3$ adopts a purely ferroelectric ground state independent of the strain amplitude, with the polarization aligned either along the constrained direction (FE$_z$ phase) for $\eta_{zz} \gtrsim +1\%$ or perpendicular to it, along one of the pseudocubic directions (FE$_x$ phase), for $\eta_{zz} \lesssim +1\%$. This prediction concerns bulklike PbTiO$_3$ under uniaxial strain. The conclusions might be different in the vicinity of surfaces that favor the appearance of AFD motions and therefore in ultrathin slabs, as previously discussed by Umeno *et al.* [35].

V. UNIAXIAL STRESS

Since it is more easily accessible experimentally, let us now consider the behavior of PbTiO$_3$ under uniaxial stress σ_{zz}. In this case, the stable phase is the one which minimizes the mechanical enthalpy $F = U - \sigma_{zz}\eta_{zz}$ (in our conventions, a positive σ_{zz} is tensile). The evolution of σ_{zz} with η_{zz} is reported in Fig. 6(a) for a few selected phases. At $\sigma_{zz} = 0$, the FE$_z$ phase shows the lowest elastic constant, which can be explained from the polarization-strain coupling.

The evolution of the mechanical enthalpy of the different phases with σ_{zz} is summarized in Fig. 6(b). We see that, like for fixed uniaxial strain, the ground state of PbTiO$_3$ under fixed uniaxial stress is always purely ferroelectric. The transition stress between the FE$_x$ and FE$_z$ phases is $\sigma_{zz} = 0$, in agreement with the fact that the common tangent between FE$_x$ and FE$_z$ curves is horizontal in the energy versus strain graph (Fig. 3). This transition stress that, at $\sigma_{zz} = 0$, the system has degenerated ground states, which corresponds to having the polarization either along z (FE$_z$ phase) or perpendicular to it (FE$_x$ phase) [53]. As expected, the presence of uniaxial tensile stresses always favors the FE$_z$ phase, while uniaxial compressive stresses always stabilizes the FE$_x$ phase. Again, under compression, the AFD$_{xy}$ + FE$_{xy}$ phase appears to be very low in energy and below the FE$_{xy}$ phase, but it is never more stable than the FE$_x$ phase.

FIG. 7. (Color online) Phase diagram of PbTiO$_3$ under uniaxial stress σ_{zz}, as predicted from LGD theory.
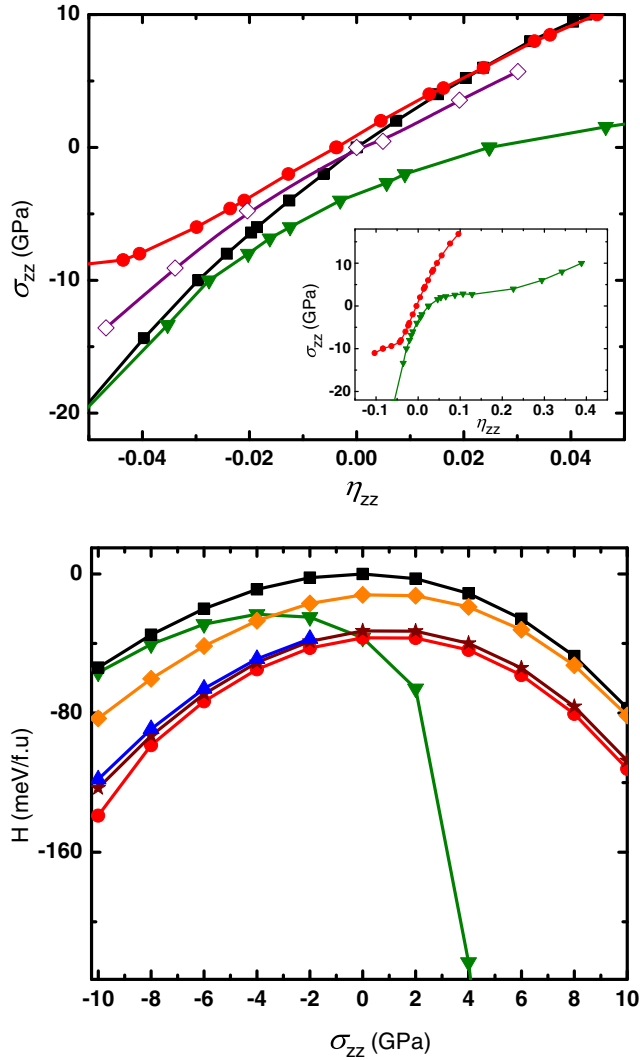
FIG. 6. (Color online) (top) Evolution of the stress (GPa) with the uniaxial strain for a few selected phases as computed within the LDA. (bottom) Mechanical enthalpy H (meV/f.u.) of different metastable phases of PbTiO$_3$ under uniaxial stress as computed within the LDA. The considered phases are as follows: PE (black squares), FE$_z$ (green downward triangles), FE$_{xy}$ (blue triangles), FE$_x$ (red circles), AFD$_{xy}$ (orange diamonds), and AFD$_{xy}$ + FE$_{xy}$ (brown stars).

Since the AFD motions does not appear to be directly involved in the ground state, the behavior of PbTiO$_3$ under uniaxial strain can be further explored using a simple Landau-Ginzburg-Devonshire (LGD) theory while including the order parameter P and neglecting the AFD degrees of freedom. The phase diagram of PbTiO$_3$ under uniaxial stress predicted from the LGD model is reported in Fig. 7. We used the parameters proposed by [54] for PbTiO$_3$, which are the same as those previously used by Qiu *et al.* [55] and similar to those of Pertsev *et al.* [14]. The phase diagram was built by minimizing the LGD potential for fixed values of σ_{33}. The LGD results are in agreement with our first-principles calculations, reproducing a FE$_x$ ground state under compressive stress and a FE$_z$ ground state under tensile stress. The phase diagram of PbTiO$_3$ under uniaxial stress is qualitatively distinct from the one reported in thin films under biaxial
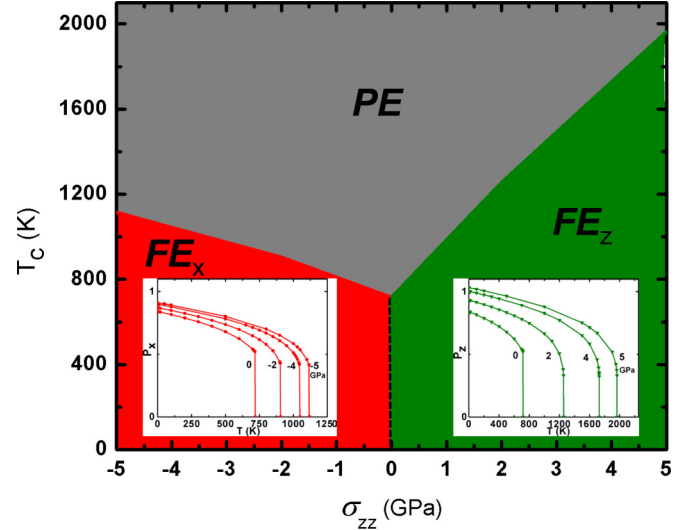
strain [14,34]. It nevertheless highlights the possibility of a stress engineering of the ferroelectric properties similar to that achieved by strain [17,19]. The uniaxial stress both increases the saturated polarization and linearly shifts the phase-transition temperature T_c to higher temperatures. The effect is particularly strong under tensile stress in the FE$_z$ phase where a stress of 1 GPa produces a T_c shift of ~300 K. We notice also that the ferroelectric phase transition tends to acquire a second-order character under tensile strain; this result is reminiscent of the observation that hydrostatic pressure also enhances the second-order character of phase transitions in ferroelectrics [56].

In Fig. 8, we report the evolution of the spontaneous polarization P_s of PbTiO$_3$ as a function of the applied uniaxial stress. Although first-principles and LGD calculations nicely agree over a wide range of compressive stress, they only coincide in the limit of small tensile stress. The first-principles calculations reveal an abrupt jump in P_s at a critical tensile stress $\sigma_{zz}^c \approx 2$ GPa that is not captured in the LGD model. This jump in the polarization of the FE$_z$ phase under tensile stress was previously highlighted by Duan *et al.* [36]. We see that a similar behavior also appears in the FE$_x$ phase under compression, but at a much larger critical stress ($\sigma_{zz}^c \approx -8$ GPa). These jumps in polarization are also accompanied by a change in the elastic constant, as observed in the stress versus strain curve (inset of Fig. 6).

As illustrated in Fig. 9, the sudden increase in P_s is linked to a dramatic jump in the c parameter and is accompanied by a strong increase in the ionic distortions. This is only partly compensated by a small decrease in the Born effective charges. This behavior (including the evolution of the atomic distortions) is totally comparable to what was previously reported for PbTiO$_3$ under isotropic negative pressure by Tinte *et al.* [58]. They explained that behavior by the proximity of a phase transition, the microscopic origin of which could be the breaking of one of the Ti-O bonds along the polar axis.

Here, this behavior appears, however, at a smaller critical tensile stress. Moreover, it is also predicted under compressive
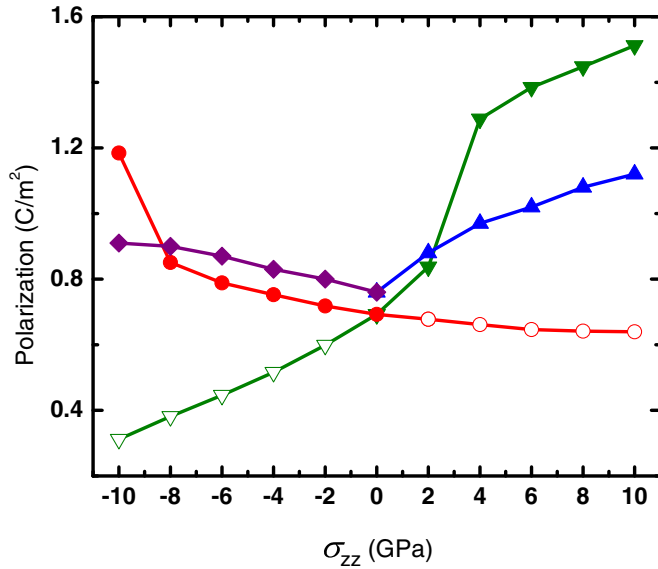
FIG. 8. (Color online) Evolution of the polarization of the FE_x (red circles) and FE_z (green downward triangles) phases of PbTiO₃ with the uniaxial stress, as predicted within the LDA. Solid symbols correspond to the region where the phase is the ground state. Purple diamonds and blue upward triangles correspond to the prediction from LGD theory at 300 K [57] for the FE_x and FE_z phases, respectively.

stress. While negative isotropic pressure is something not practically accessible experimentally, uniaxial stresses (both tensile or compressive) were recently made accessible to laboratory-on-a-chip experiments [59–61]. This experiment could offer the possibility to confirm our prediction experimentally. Moreover, it could also reveal to be of concrete practical interest: as highlighted by Duan *et al.* [36], in the vicinity of the critical stress, PbTiO₃ will exhibit a large piezoelectric response, i.e., $d_{zzz} = \partial P_z / \partial \sigma_{zz}$ $(d_{xzz} = \partial P_x / \partial \sigma_{zz})$, that is proportional to the slope of P in Fig. 8 that might be directly exploited to enlarge the piezoelectric sensitivity of nanodevices.

VI. CONCLUSIONS

The behavior of bulk PbTiO₃ under uniaxial strains and stresses has been explored from first-principles calculations and LGD theory. Under uniaxial strain, PbTiO₃ adopts a purely ferroelectric FE_x ground state under compressive strain and switches to a purely ferroelectric FE_z ground state under tensile strain larger than $\eta_{zz}^c \approx 1\%$. This behavior is in contrast to the emergence of phases combining FE and AFD distortion under biaxial strain and isotropic pressure. The situation might be different in the vicinity of surfaces that promote AFD distortions and therefore in ultrathin films [35]. Under uniaxial stress, PbTiO₃ exhibits either a FE_x ground state under compression or a FE_z ground state under tension. Moreover, our calculations highlight an abrupt jump in the structural parameters under both compressive and tensile stresses at the critical values $\sigma_{zz} \approx +2$ and -8 GPa. While LGD theory reproduces nicely the first-principles data, it does not capture this strong relaxation and so remains only valid in a region between the critical stresses. The jump in the structural
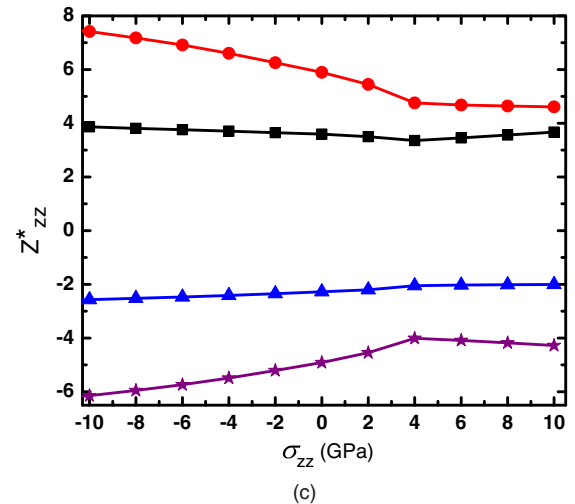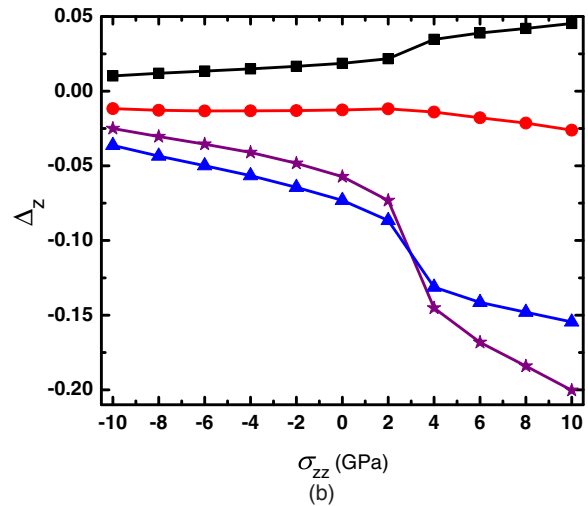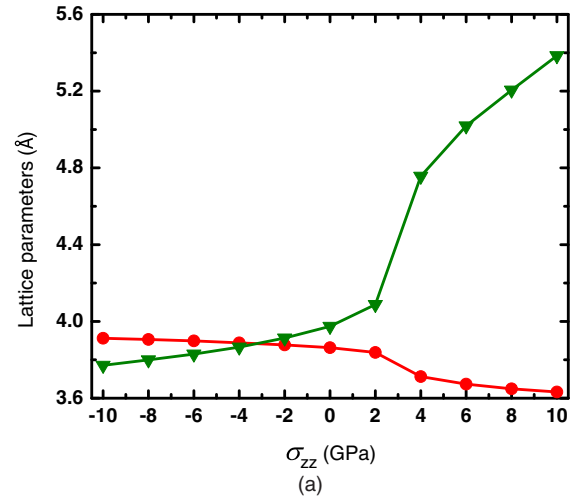

FIG. 9. (Color online) Evolution of (a) the c (green triangles) and a (red circles) lattice parameters (Å), (b) atomic displacements, and (c) Born effective charges as a function of uniaxial stress in the FE_z phase of PbTiO₃ as calculated within the LDA. In (b) and (c) black squares are for Pb, red circles are for Ti, purple stars are for O_1, and blue triangles are for $O_{2,3}$.

parameters is linked to a strong increase in the piezoelectric response, which might potentially be exploited. We hope that

our work will motivate further experimental characterization of $PbTiO_3$ under uniaxial tensile and compressive stresses.

ACKNOWLEDGMENTS

[1] M. E. Lines and A. M. Glass, *Principles and Applications of Ferroelectrics and Related Materials* (Clarendon, Oxford, 1977).

[2] R. E. Cohen, Nature (London) **358**, 136 (1992).

[3] Ph. Ghosez, E. Cockayne, U. V. Waghmare, and K. M. Rabe, Phys. Rev. B **60**, 836 (1999).

[4] J. C. Wojdel, P. Hermet, M. P. Ljungberg, Ph. Ghosez, and J. Iniguez, J. Phys. Condens. Matter **25**, 305401 (2013).

[5] C. Bungaro and K. M. Rabe, Phys. Rev. B **71**, 035420 (2005).

[6] K. M. Rabe and Ph. Ghosez, Top. Appl. Phys. **105**, 111 (2007).

[7] I. A. Kornev, L. Bellaiche, P. Bouvier, P.-E. Janolin, B. Dkhil, and J. Kreisel, Phys. Rev. Lett. **95**, 196804 (2005).

[8] E. Bousquet and Ph. Ghosez, Phys. Rev. B **74**, 180101 (2006).

[9] P.-E. Janolin, P. Bouvier, J. Kreisel, P. A. Thomas, I. A. Kornev, L. Bellaiche, W. Crichton, M. Hanfland, and B. Dkhil, Phys. Rev. Lett. **101**, 237601 (2008).

[10] M. Dawber, K. M. Rabe, and J. F. Scott, Rev. Mod. Phys. **77**, 1083 (2005).

[11] K. M. Rabe, Curr. Opin. Solid State Mater. Sci. **9**, 122 (2005).

[12] J. Junquera and Ph. Ghosez, J. Comput. Theor. Nanosci. **5**, 2071 (2008).

[13] D. G. Schlom, L. Q. Chen, C. B. Eom, K. M. Rabe, S. K. Streiffer, and J. M. Triscone, Annu. Rev. Mater. Res. **37**, 589 (2007).

[14] N. A. Pertsev, A. G. Zembilgotov, and A. K. Tagantsev, Phys. Rev. Lett. **80**, 1988 (1998).

[15] N. A. Pertsev, A. K. Tagantsev, and N. Setter, Phys. Rev. B **61**, R825 (2000).

[16] O. Diéguez, K. M. Rabe, and D. Vanderbilt, Phys. Rev. B **72**, 144101 (2005).

[17] K. J. Choi, M. Biegalski, Y. L. Li, A. Sharan, J. Schubert, R. Uecker, P. Reiche, Y. B. Chen, X. Q. Pan, V. Gopalan, L.-Q. Chen, D. G. Schlom, and C. B. Eom, Science **306**, 1005 (2004).

[18] A. Vasudevarao, A. Kumar, L. Tian, J. H. Haeni, Y. L. Li, C.-J. Eklund, Q. X. Jia, R. Uecker, P. Reiche, K. M. Rabe, L. Q. Chen, D. G. Schlom, and V. Gopalan, Phys. Rev. Lett. **97**, 257602 (2006).

[19] J. H. Haeni, P. Irvin, W. Chang, R. Uecker, P. Reiche, Y. L. Li, S. Choudhury, W. Tian, M. E. Hawley, B. Craigo, A. K. Tagantsev, X. Q. Pan, S. K. Streiffer, L. Q. Chen, S. W. Kirchoefer, J. Levy, and D. G. Schlom, Nature (London) **430**, 758 (2004).

[20] T. Birol, N. A. Benedek, H. Das, A. Wysocki, A. T. Mulder, B. M. Abbett, E. H. Smith, S. Ghosh, and C. J. Fennie, Curr. Opin. Solid State Mater. Sci. **16**, 227 (2012).

[21] S. Bhattacharjee, E. Bousquet, and Ph. Ghosez, Phys. Rev. Lett. **102**, 117602 (2009).

[22] T. Günter, E. Bousquet, A. David, Ph. Boullay, Ph. Ghosez, W. Prellier and M. Fiebig, Phys. Rev. B **85**, 214120 (2012).

[23] E. Bousquet, N. A. Spaldin, and Ph. Ghosez, Phys. Rev. Lett. **104**, 037601 (2010).

[24] O. Diéguez, O. E. González-Vázquez, J. C. Wojdel, and J. Íñiguez, Phys. Rev. B **83**, 094105 (2011).

[25] C. Escorihuela-Sayalero, O. Diéguez, and J. Íñiguez, Phys. Rev. Lett. **109**, 247202 (2012).

[26] Y. Yang, W. Ren, M. Stengel, X. H. Yan, and L. Bellaiche, Phys. Rev. Lett. **109**, 057602 (2012).

[27] C. J. Fennie and K. M. Rabe, Phys. Rev. Lett. **97**, 267602 (2006).

[28] J. H. Lee and K. M. Rabe, Phys. Rev. Lett. **104**, 207204 (2010).

[29] E. Bousquet, Ph.D. thesis, Université de Liège, 2008, http://bictel.ulg.ac.be/ETD-db/collection/available/ULgetd-03232009-095839/unrestricted/thesis_Bousquet.pdf.

[30] J. L. Blok, D. H. A. Blank, G. Rijnders, K. M. Rabe, and D. Vanderbilt, Phys. Rev. B **84**, 205413 (2011).

[31] Y. Yang, M. Stengel, W. Ren, X. H. Yan, and L. Bellaiche, Phys. Rev. B **86**, 144114 (2012).

[32] A. M. Glazer, Acta Crystallogr., Sect. B **28**, 3384 (1972).

[33] C. J. Howard and H. T. Stokes, Acta Crystallogr., Sect. B **54**, 782 (1998); **58**, 565 (2002).

[34] A. Yu. Emelyanov, N. A. Pertsev, and A. L. Kholkin, Phys. Rev. B **66**, 214108 (2002).

[35] Y. Umeno, T. Shimada, T. Kitamura, and Ch. Elsässer, Phys. Rev. B **74**, 174111 (2006).

[36] Y. Duan, H. Shi, and L. Qin, J. Phys. Condens. Matter **20**, 175210 (2008).

[37] M. Guennou, P. Bouvier, G. S. Chen, B. Dkhil, R. Haumont, G. Garbarino, and J. Kreisel, Phys. Rev. B **84**, 174107 (2011).

[38] M. Guennou, P. Bouvier, P. Toulemonde, C. Darie, C. Goujon, P. Bordet, M. Hanfland, and J. Kreisel, Phys. Rev. Lett. **112**, 075501 (2014).

[39] X. Gonze, J.-M. Beuken, R. Caracas, F. Detraux, M. Fuchs, G.-M. Rignanese, L. Sindic, M. Verstraete, G. Zerah, F. Jollet, M. Torrent, A. Roy, M. Mikami, Ph. Ghosez, J.-Y. Raty, and D. C. Allan, Comput. Mater. Sci. **25**, 478 (2002).

[40] X. Gonze, G.-M. Rignanese, M. Verstraete, J.-M. Beuken, Y. Pouillon, R. Caracas, F. Jollet, M. Torrent, G. Zerah, M. Mikami, Ph. Ghosez, M. Veithen, V. Olevano, L. Reining, R. Godby, G. Onida, D. Hamann, and D. C. Allan, Zeitschrift fuer Kristallographie **220**, 558 (2005).

[41] X. Gonze *et al.*, Comput. Phys. Commun. **180**, 2582 (2009).

[42] S. Goedecker, M. Teter, and J. Hutter, Phys. Rev. B **54**, 1703 (1996).

[43] M. Teter, Phys. Rev. B **48**, 5031 (1993).

[44] Z. Wu and R. E. Cohen, Phys. Rev. B **73**, 235116 (2006).

[45] A. M. Rappe, K. M. Rabe, E. Kaxiras, and J. D. Joannopoulos, Phys. Rev. B **41**, 1227 (1990).

[46] See the OPIUM website at http://opium.sourceforge.net/.

[47] X. Gonze and C. Lee, Phys. Rev. B **55**, 10355 (1997).

[48] R. D. King-Smith and D. Vanderbilt, Phys. Rev. B **47**, 1651(R) (1993).

[49] G. Shirane, H. Danner, and P. Pepinsky, Phys. Rev. **105**, 856 (1957).

[50] Tetragonal lattice constants of PbTiO$_3$ extrapolated to 0 K are from S. A. Mabud and A. M. Glazer, J. Appl. Cryst. **12**, 49 (1979). Spontaneous polarization is from V. G. Gavrilyachenko, R. I. Spinko, M. A. Martynen, and R. G. Fesenko, Sov. Phys. Solid State **12**, 1203 (1970).

[51] Relaxations with a polarization developing along the three directions of space have also been performed but relaxed back to FE$_x$ or FE$_z$ phases, except in the vicinity of $\eta_{zz} = 0$, and in that case, they always produce a lower gain in energy than the FE$_x$ or FE$_z$ configurations.

[52] The spontaneous polarization was also estimated by multiplying the atomic displacements by the Born effective charges of either the reference cubic phase or of the relaxed FE phase at each stress. The Berry phase calculation is much closer to the estimate.

[53] This degeneracy manifests in Fig. 3 as a horizontal common tangent between the FE$_x$ and FE$_z$ curves.

[54] M. J. Haun, Z. Q. Zhuang, E. Furman, S. J. Jang, and L. E. Cross, Ferroelectrics **99**, 45 (1989).

[55] Q. Y. Qiu, R. Mahjoub, S. P. Alpay, and V. Nagarajan, Acta Mater. **58**, 823 (2010).

[56] P. Pruzan, D. Gourdain, and J. C. Chervin, Phase Transitions **80**, 1103 (2007).

[57] The LGD model predicts a very similar evolution at low temperatures but with a slightly larger amplitude. Since LDA tends to slightly underestimate the polarization, we have made the comparison with LGD theory at 300 K.

[58] S. Tinte, K. M. Rabe, and D. Vanderbilt, Phys. Rev. B **68**, 144105 (2003).

[59] D. Fabrègue, N. Andrè, M. Coulombier, J.-P. Raskin, and T. Pardoen, Micro Nanolett **2**, 13 (2007).

[60] S. Gravier, M. Coulombier, A. Safi, N. Andrè, A. Boe, J.-P. Raskin, and T. Pardoen, J. Microelectromech. Syst. **18**, 555 (2009).

[61] U. K. Bhaskar, T. Pardoen, V. Passi, and J.-P. Raskin, Appl. Phys. Lett. **102**, 031911 (2013).